



### AperTO - Archivio Istituzionale Open Access dell'Università di Torino

# Are the large filamentous microfossils preserved in Messinian gypsum colorless sulfide-oxidizing bacteria?

This is the author's manuscript	
Original Citation:	
Availability:	
This version is available http://hdl.handle.net/2318/1525226	since 2018-07-17T16:02:04Z
Published version:	
DOI:10.1130/G37018.1	
Terms of use:	
Open Access	
Anyone can freely access the full text of works made available as under a Creative Commons license can be used according to the t of all other works requires consent of the right holder (author or p protection by the applicable law.	erms and conditions of said license. Use

(Article begins on next page)

- Are the large filamentous microfossils preserved in
- 2 Messinian gypsum colorless sulfide-oxidizing bacteria?
- 3 Francesco Dela Pierre<sup>1\*</sup>, Marcello Natalicchio<sup>1</sup>, Simona Ferrando<sup>1</sup>, Roberto
- 4 Giustetto<sup>1</sup>, Daniel Birgel<sup>2</sup>, Giorgio Carnevale<sup>1</sup>, Susanne Gier<sup>2</sup>, Francesca Lozar<sup>1</sup>,
- 5 Domenica Marabello<sup>3</sup>, and Jörn Peckmann<sup>2,4</sup>
- 6 <sup>1</sup>Dipartimento di Scienze della Terra, Università di Torino, 10125 Torino, Italy
- 7 <sup>2</sup>Department für Geodynamik und Sedimentologie, Universität Wien, 1090 Wien, Austria
- 8 <sup>3</sup>Dipartimento di Chimica, Università di Torino, 10125 Torino, Italy
- 9 <sup>4</sup>Institut für Geologie, Universität Hamburg, 20146 Hamburg, Germany
- 10 \*E-mail: francesco.delapierre@unito.it

### 11 **ABSTRACT**

12

13

14

15

16

17

18

19

20

21

22

The thick gypsum deposits formed in the Mediterranean basin during the Messinian salinity crisis incorporate dense mazes of filamentous fossils, which were interpreted as algae or cyanobacteria, thus pointing to a shallow marine subtidal or intertidal environment. The data presented herein reveal that these filaments rather represent remains of colorless, vacuolated sulfide-oxidizing bacteria. This interpretation is supported by the presence of small crystal aggregates of iron sulfide (pyrite) and associated polysulfide within the filamentous fossils. Pyrite and polysulfide are considered to result from early diagenetic transformation of original zero-valent sulfur globules stored within the cells, which is a clade-diagnostic feature of living and degraded sulfur bacteria. Besides filamentous fossils, the studied gypsum crystals contain remains of eury- and stenohaline diatoms and clay-rich aggregates interpreted as

alteration products of marine snow floccules. This peculiar fossil assemblage reflects conditions of increased productivity in the water column, which was triggered by high fluxes of nutrients into the basin during phases of enhanced riverine runoff and fresh water discharge. This study confirms that gypsum evaporites have great potential to preserve the early stages of the taphonomic alteration of bacterial cells, shedding light on the paleoecology of ancient hypersaline environments.

### **INTRODUCTION**

23

24

25

26

27

28

29

30

31

32

33

34

35

36

37

38

39

40

41

42

43

44

45

Being able to tolerate extreme, hypersaline conditions, prokaryotes are often the only fossils found in evaporites (Warren, 2010). The prokaryote remains are commonly exceptionally well-preserved because of fast and early growth of the evaporite minerals, allowing for the rapid entombment of cells (Lugli et al., 2010). Well known examples of fossiliferous evaporites are the thick gypsum sequences associated with halite and anhydrite that were deposited in the Mediterranean basin ~6 m.y. ago during the Messinian salinity crisis (MSC; Roveri et al., 2014). The Messinian gypsum incorporates dense mazes of filamentous fossils, which were originally interpreted as remains of benthic algae (Vai and Ricci Lucchi, 1977) or cyanobacteria (Rouchy and Monty, 2000). Should this assignment be correct, the depositional setting must have been shallow, situated within the photic zone. The extraction and amplification of cyanobacterial ribosomal RNA from filament-bearing gypsum from Italy supported this interpretation (Panieri et al., 2010). However, based on comparison with modern bacteria, Schopf et al. (2012) suggested that the filamentous fossils represent remains of colorless sulfideoxidizing bacteria such as Beggiatoa and Thioploca. Similar filamentous fossils preserved in other lithologies than gypsum including chert (Schopf et al., 2015),

46	phosphorite (Bailey et al., 2013), and limestone (Peckmann et al., 2004) have previously
47	been interpreted as members of the colorless sulfur bacteria. Here we present a
48	petrographic, minerochemical, and Raman spectroscopy study of the fossiliferous
49	gypsum from the Primary Lower Gypsum unit of the Piedmont Basin (northwest Italy;
50	Fig. 1), focusing on the abundant filamentous fossils. The new results indicate that these
51	enigmatic fossils are more likely to represent sulfur bacteria, agreeing with recent
52	interpretations of the environmental conditions during the deposition of the Messinian
53	gypsum.
54	THE PRIMARY LOWER GYPSUM UNIT
55	The Primary Lower Gypsum unit formed during the first stage of the MSC (5.97-
56	5.60 Ma) in silled peripheral sub-basins of the Mediterranean (Roveri et al., 2014). The
57	depth of these sub-basins is still a matter of discussion. As elsewhere in the
58	Mediterranean, this unit shows a striking lithological cyclicity in the Piedmont Basin,
59	defined by rhythmic alternation of shale and gypsum couplets. This cyclicity is
60	interpreted to reflect precession-controlled humid (shale) to arid (gypsum) climate
61	oscillations (Dela Pierre et al., 2014). The gypsum layers studied herein, up to 30 m thick
62	(Fig. 2A), belong to the lowermost four cycles and are composed of dm-sized vertically
63	oriented twinned selenite crystals (swallow-tail twins). The crystals nucleated at the
64	sediment-brine interface with their vertical orientation reflecting competitive growth in a
65	relatively deep basin permanently covered by brines (Lugli et al., 2010).
66	METHODS
67	Petrographic sections of 20 samples collected from three outcrops were studied
68	under an optical microscope and analyzed for their ultraviolet (UV) fluorescence (for

details see the GSA Data Repository<sup>1</sup>). Five representative samples were studied with a scanning electron microscope (SEM) coupled with an energy-dispersive X-ray spectrometer (EDS) and a Raman spectrometer. Three samples were dissolved in ultrapure water and the resulting residue and isolated fragments were analyzed by light microscopy, electron microscopy with coupled energy-dispersive X-ray spectroscopy, and microRaman. X-ray diffraction (XRD) analyses were performed on isolated filaments after dissolution.

#### THE GYPSUM FILAMENTOUS FOSSILS

69

70

71

72

73

74

75

76

77

78

79

80

81

82

83

84

85

86

87

88

89

90

91

The studied swallow-tail twins of gypsum display an internal lamination in the reentrant angles marked by the rhythmic repetition of mm-thick clear and turbid laminae (Fig. 2B), possibly representing short term (annual?) climate oscillations between more humid (turbid lamina) and more arid (clear lamina) conditions. In the clear laminae solid inclusions are scarce or absent, whereas they are abundant in the turbid laminae. They include (1) rare stenohaline (*Navicula* sp., *Trigonium* sp.) and euryhaline (*Surirella* sp.) diatoms (Fig. 2C; Natalicchio et al., 2014), and (2) loosely packed, fluorescent clay-rich aggregates up to 500 µm across and locally containing altered diatom frustules. Similar aggregates have already been reported from the shale layers interbedded with the gypsum and have been interpreted to represent marine snow floccules that originated by aggregation of clay and diatoms in the overlying water column during episodes of eutrophication and phytoplankton bloom (Dela Pierre et al., 2014). Other solid inclusions are (3) silt-sized terrigenous material (mica flakes and detrital mineral grains; Fig. DR2 in the Data Repository), and (4) curved and straight filaments (Figs. 2D and 2F). The filaments are up to 2 mm long and 60–80 µm across, showing a rather uniform diameter

### Publisher: GSA Journal: GEOL: Geology

DOI:10.1130/G37018.1

throughout their length. All filaments are fluorescent when exposed to UV light (Fig. 2E),
suggesting a high content of organic matter. While the filaments are mostly observed in
the re-entrant angle of the crystals, they are also found on vertical growth bands with
their long axis aligned to former crystal surfaces (Fig. 2D). All filaments are preserved as
hollow tubes in the gypsum (Fig. 2F). Well-preserved ones are made of a sequence of
cellular compartments of uniform shape and size (Fig. 2G). The surface of the filaments
displays an irregular honey-comb structure (Fig. 2H; Fig. DR1), which—according to
XRD data (Fig. DR4)—consists of clay minerals of the smectite group and traces of illite.
The elemental composition of the clay minerals falls between the compositional fields of
nontronite and montmorillonite (Fig. DR3), confirming the presence of smectite minerals.
The composition of the smectite clay minerals is distinguishable from that of the detrital
micas (Fig. DR2), which represent muscovite, phengite, and accessory Fe-Mg chlorite
(Fig. DR3; Table DR1). The identification of clay minerals by micro-Raman was
precluded due to their weak Raman scattering and the fluorescence of the filaments.
However, micro-Raman revealed the scattered presence of carbonaceous material (Fig.
3), possibly representing a remnant of the original biomass of the filamentous organisms.
Some filaments are coated by a layer of anhedral dolomite microcrystals (2–5 $\mu m$
across), which reveal a partially hollow core (Figs. 2I and 2J). The dolomite crystals
apparently grew on the outer surfaces of filaments within a clayey matrix before the final
incorporation of filaments within gypsum. In all studied samples, the filaments contain
opaque, subspherical grains that are $1-2~\mu m$ across (Fig. 2E), which were identified as
iron sulfides by SEM-EDS and XRD. MicroRaman analyses identified the iron sulfides
as aggregates of microcrystalline pyrite, revealing characteristic peaks at ~340, 376, and

# Journal: GEOL: Geology DOI:10.1130/G37018.1

426 cm<sup>-1</sup> (Fig. 3; see the Data Repository). In rare cases, a broad band at ~470 cm<sup>-1</sup> was observed (Fig. 3), which is best explained by the presence of polysulfide (S<sub>n</sub><sup>2-</sup>) that shows similar bands in the 440 and 480 cm<sup>-1</sup> wavelength region (main at 470; Berg et al., 2014).

#### THE NATURE OF THE FILAMENTOUS FOSSILS

119

120

121

122

123

124

125

126

127

128

129

130

131

132

133

134

135

136

137

The fact that the filaments were also observed along the vertical growth bands besides in the re-entrant angle of the crystals suggests that the microorganisms lived adhering to the crystal faces, thus representing fossils of benthic biota. After having being interpreted as fossils of algae (Vai and Ricci Lucchi, 1977) or cyanobacteria (Rouchy and Monty, 2000; Panieri et al., 2010), Schopf et al. (2012) suggested that the filamentous fossils represent remains of sulfide-oxidizing bacteria. The colorless, vacuolated sulfideoxidizing bacteria like *Beggiatoa* and *Thioploca* oxidize hydrogen sulfide to sulfate with oxygen or nitrate, thus, requiring steep redox gradients and preferring microoxic environments (Schulz and Jørgensen, 2001). These and other closely related Gammaproteobacteria are able to grow to enormous sizes where the concentrations of their substrates are high enough to overcome size limitations posed by molecular diffusion (Schulz and Jørgensen, 2001). Such conditions are found in upwelling areas, silled basins, eutrophic lakes and bays, at hydrothermal vents, or at methane seeps (Schulz and Jørgensen, 2001). Different strains and populations of *Beggiatoa*, for example, reveal a range of filament widths from below 1–200 µm (Teske and Nelson, 2006). None of the studied Messinian filaments have the tapered ends that are observed in some *Thioploca* (Jørgensen and Gallardo, 1999), but this is no argument to exclude this genus, since tapering is not found in all of its members. The multicellular filaments

### Publisher: GSA Journal: GEOL: Geology

DOI:10.1130/G37018.1

may consist of a row of hundreds to a thousand disk-snaped cells and reach a length of
several centimeters (Teske and Nelson, 2006). Consequently, the shape, the size, and the
apparent segmentation (Fig. 2G) of the Messinian filaments agree with an assignment to
the colorless sulfur bacteria. The presence of carbonaceous material in the filaments is of
course not diagnostic for a group of prokaryotes, but is in accord with a biogenic origin.
The recognition of dolomite coatings is remarkable, since early dolomite formation has
been found to be driven by bacterial sulfate reduction (e.g., Vasconcelos et al., 1995).
Dolomite formation occurred before the filaments were entombed by gypsum. The
paleoenvironment was consequently conducive to dolomite formation; precipitation may
have exclusively occurred post-mortem, but must have been a very early taphonomic
process. Interestingly, some <i>Thioploca</i> benefit from the local production of hydrogen
sulfide by sulfate-reducing bacteria of the genus Desulfonema, which grow on the outer
surface of the <i>Thioploca</i> sheaths (Fukui et al., 1999). Such an association of sulfate
reducers adhering to the filamentous sulfide oxidizers can explain the observed dolomite
coatings.
A diagnostic feature of modern colorless sulfur bacteria is the presence of zero-
valent sulfur globules stored within membrane-bounded vesicles, which represent an
intermediate product of the oxidation of sulfide to sulfate (Teske and Nelson, 2006).
Similar sulfur-rich inclusions are present in the microfossils studied here. Remarkably,
colorless sulfur bacteria can sometimes retain elemental sulfur in the sheath after cell
death and loss of cytoplasm (Bailey et al., 2013). Although no isolated elemental sulfur
was detected, we observed aggregates of microcrystalline pyrite and associated
polysulfide. The chemical nature of the sulfur stored by modern prokaryotes is

### Publisher: GSA Journal: GEOL: Geology

## DOI:10.1130/G37018.1

161

162

163

164

165

166

167

168

169

170

171

172

173

174

175

176

177

178

179

180

181

182

183

controversially discussed (Berg et al., 2014). Raman data indicate that this sulfur is extremely fine-grained and arranged in a stable S8 ring configuration (Pasteris et al., 2001). Recently also polysulfide, possibly derived from the transformation of cyclooctosulfur, was reported in some *Beggiatoa* cultures (Berg et al., 2014). Therefore, the presence of polysulfide in the Messinian filaments is of interest. It may represent a remnant of elemental sulfur stored by the bacteria. The majority of the sulfur, however, reacted with iron, fostering the formation of pyrite (Berner, 1984). It is difficult to exclude that the polysulfide resulted from the reoxidation of pyrite during weathering, but the otherwise excellent preservation of the fossils in gypsum crystals—sealing off the solid inclusions from external influences—may be taken as an argument for a primary origin of polysulfide. Although the Messinian filaments are unusually large for prokaryotes, bacteria other than colorless sulfur bacteria cannot be excluded based on size and shape alone. Some oscillatoriacean cyanobacteria, with sheaths up to 100 µm in diameter (Demoulin and Janssen, 1981) are virtually indistinguishable from colorless sulfur bacteria based solely on morphology. In Messinian gypsum from the Monte Tondo quarry, filaments with a width of up to 70 µm have been recognized by Schopf et al. (2012), which tempted the authors to suggest that the filaments were sulfur bacteria rather than cyanobacteria. Panieri et al. (2010) documented a range of diameters from 20 to 30 µm for filaments from the same quarry, which had been interpreted as cyanobacteria based on the extraction of ribosomal RNA from the gypsum. However, it cannot be excluded that this genetic material derived from planktic microorganisms that sunk to the seafloor (see Lugli et al., 2010) or from subrecent or recent endolithic cyanobacteria (cf. Ziolkowski et

# Journal: GEOL: Geology DOI:10.1130/G37018.1

al., 2013). Another group that could be considered as producers of the filaments are ironoxidizing bacteria. Interestingly, the mineral composition of the filaments, which is clearly different from that of the associated detrital micas, is consistent with microbially-mediated clay authigenesis (cf. Konhauser and Urrutia, 1999). Chamosite and illite are typical products of this process, but smectites (particularly nontronite) are also found (Ueshima and Tazaki, 2001). Unfortunately, the mineralogy of the studied filaments is not diagnostic of a particular group of bacteria (cf. Konhauser and Urrutia, 1999). However, in an environment that sustained bacterial iron oxidation, the nucleation of clays with high iron contents ought to be expected (cf. Peckmann et al., 2008). The absence of such clay minerals argues against an assignment of the Messinian filaments to iron-oxidizing bacteria. Such an attribution is further unlikely, because known filamentous iron oxidizers are much smaller than the studied filaments (5–6 µm; Crosby et al., 2014). Based on the different lines of evidence, we interpret the filaments preserved in Messinian gypsum as fossils of colorless sulfide-oxidizing bacteria.

### IMPLICATIONS FOR MESSINIAN GYPSUM DEPOSITION

Modern colorless sulfur bacteria occur in a wide range of water depths from bathyal to peritidal settings (Bailey et al., 2009) and show a phobic response to light (Nelson and Castenholz, 1982). The assignment of the Messinian filaments to this group of bacteria indicates that the gypsum locally formed at greater water depth than previously suggested, which was partly based on the assumption that the filaments reflect benthic phototrophs. The revised scenario agrees with the findings of Ochoa et al. (2015), who reported that gypsum deposition was not limited to shallow depth. The large sulfur bacteria inhabit diverse environments, including those in which bacterial sulfate

### Journal: GEOL: Geology DOI:10.1130/G37018.1

207

208

209

210

211

213

214

215

216

217

218

219

220

221

222

223

224

225

226

227

228

reduction produces hydrogen sulfide in organic-rich sediments (Teske and Nelson, 2006). Deposition of organic-rich sediments, commonly containing abundant diatoms and marine snow floccules, is favored by eutrophication of the water column caused by increased nutrient influx in the course of enhanced riverine runoff (Graco et al., 2001). And indeed, recent work confirms that the early stages of the MSC were typified by algal 212 blooms caused by eutrophication (Dela Pierre et al., 2014). Similarly, a local increase of riverine runoff has been demonstrated for the early stage of the MSC by gypsum fluid inclusion data, indicating influx of sulfate-rich waters that mixed with seawater (Natalicchio et al. 2014). The algal blooms enhanced organic matter degradation by bacterial sulfate reduction in an oxygen-depleted sedimentary environment, which provided the high hydrogen sulfide flux required for the growth of colorless sulfur bacteria. A steep gradient between anoxic, sulfide-rich sediments and oxygen-depleted but probably nitrate-rich bottom water supposedly favored these bacteria. Such an eutrophication scenario agrees with our reinterpretation of the Messinian filaments as sulfide-oxidizing bacteria, similar to those that are found in association with diatoms and marine snow floccules in modern eutrophic settings. **ACKNOWLEDGMENTS** This research was funded with University of Torino 2013 funds (ex 60% grant to Dela Pierre). B.C Schreiber is thanked for comments on an early draft of the manuscript. The Editor J.A. Spotila, and referees J. Bailey, E. Jagniecki, and W. Krijgsman are thanked for their careful and throughout reviews. REFERENCES CITED

# Journal: GEOL: Geology DOI:10.1130/G37018.1 , S.B., and Corsetti, F., 2009. Chemotrophic microbial

229	Bailey, J.V., Orphan, V.J., Joye, S.B., and Corsetti, F., 2009, Chemotrophic microbial
230	mats and their potential for preservation in the rock record: Astrobiology, v. 9,
231	p. 843–859, doi:10.1089/ast.2008.0314.
232	Bailey, J.V., Corsetti, F.A., Greene, S.E., Crosby, C.H., Liu, P., and Orphan, V.J., 2013,
233	Filamentous sulfur bacteria preserved in modern and ancient phosphatic sediments:
234	Implications for the role of oxygen and bacteria in phosphogenesis: Geobiology,
235	v. 11, p. 397–405, doi:10.1111/gbi.12046.
236	Berg, J.S., Schwedt, A., Kreutzmann, A.C., Kuypers, M.M.M., and Milucka, J., 2014,
237	Polysulfides as intermediates in the oxidation of sulfide to sulfate by Beggiatoa spp:
238	Applied and Environmental Microbiology, v. 80, p. 629-636,
239	doi:10.1128/AEM.02852-13.
240	Berner, R.A., 1984, Sedimentary pyrite formation: an update: Geochimica et
241	Cosmochimica Acta, v. 48, p. 605–615, doi:10.1016/0016-7037(84)90089-9.
242	Crosby, C.H., Bailey, J.V., and Shrama, M., 2014, Fossil evidence of iron-oxidizing
243	chemolithotrophy linked to phosphogenesis in the wake of the Great Oxidation
244	Event: Geology, v. 42, p. 1015-1018, doi:10.1130/G35922.1.
245	Dela Pierre, F., Clari, P., Natalicchio, M., Ferrando, S., Giustetto, R., Lozar, F., Lugli, S.,
246	Manzi, V., Roveri, M., and Violanti, D., 2014, Flocculent layers and bacterial mats
247	in the mudstone interbeds of the Primary Lower Gypsum Unit (Tertiary Piedmont
248	Basin, NW Italy): Archives of palaeoenvironmental changes during the Messinian
249	salinity crisis: Marine Geology, v. 355, p. 71–87, doi:10.1016/j.margeo.2014.05.010.

# Journal: GEOL: Geology DOI:10.1130/G37018.1 Demoulin, V., and Janssen, M.P., 1981. Relationship between diameter of the filament

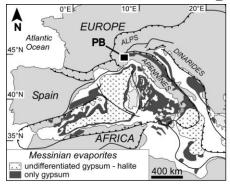
250	Demoulin, V., and Janssen, M.P., 1981, Relationship between diameter of the filament
251	and cell shape in blue-green algae: British Phycological Journal, v. 16, p. 55-58,
252	doi:10.1080/00071618100650051.
253	Fukui, M., Teske, A., Aßmus, B., Muzyer, G., and Widdel, F., 1999, Physiology,
254	phylogenetic relationships, and ecology of filamentous sulfate-reducing bacteria
255	(genus Desulfonema): Archives of Microbiology, v. 172, p. 193-203,
256	doi:10.1007/s002030050760.
257	Graco, M., Farìas, L., Molina, V., Guitiérrez, D., and Nielsen, L.P., 2001, Massive
258	developments of microbial mats following phytoplankton blooms in a naturally
259	eutrophic bay: Implications for nitrogen cycling: Limnology and Oceanography,
260	v. 46, p. 821–832, doi:10.4319/lo.2001.46.4.0821.
261	Jørgensen, B.B., and Gallardo, V.A., 1999, <i>Thioploca</i> spp.: Filamentous sulfur bacteria
262	with nitrate vacuoles: FEMS Microbiology Ecology, v. 28, p. 301–313,
263	doi:10.1016/S0168-6496(98)00122-6.
264	Konhauser, K.O., and Urrutia, M.M., 1999, Bacterial clay authigenesis: A common
265	biogeochemical process: Chemical Geology, v. 161, p. 399–413, doi:10.1016/S0009-
266	2541(99)00118-7.
267	Lugli, S., Manzi, V., Roveri, M., and Schreiber, B.C., 2010, The Primary Lower Gypsum
268	in the Mediterranean: A new facies interpretation for the first stage of the Messinian
269	salinity crisis: Palaeogeography, Palaeoclimatology, Palaeoecology, v. 297, p. 83-
270	99, doi:10.1016/j.palaeo.2010.07.017.
271	Natalicchio, M., Dela Pierre, F., Lugli, S., Lowenstein, T.K., Feiner, S.J., Ferrando, S.,
272	Manzi, V., Roveri, M., and Clari, P., 2014, Did late Miocene (Messinian) gypsum

273	precipitate from evaporated marine brines? Insight from the Piedmont Basin (Italy):
274	Geology, v. 42, p. 179–182, doi:10.1130/G34986.1.
275	Nelson, DC, and Castenholz, RW, 1982, Light response of Beggiatoa: Archives of
276	Microbiology, v. 131, p. 146–155, doi: 10.1007/BF01053997.
277	Ochoa, D., Sierro, F.J, Lofi, J., Maillard, A., Flores, J, and Suàrez, M., 2015,
278	Synchronous onset of the Messinian evaporite precipitation: First Mediterranean
279	offshore evidence: Earth and Planetary Science Letters, v. 427, p. 112–124, doi:
280	10.1016/J.epsl.2015.06.059.
281	Panieri, G., Lugli, S., Manzi, V., Roveri, M., Schreiber, C.B., and Palinska, K.A., 2010,
282	Ribosomal RNA gene fragments from fossilized cyanobacteria identified in primary
283	gypsum from the late Miocene, Italy: Geobiology, v. 8, p. 101-111,
284	doi:10.1111/j.1472-4669.2009.00230.x.
285	Pasteris, J.D., Freeman, J.J., Goffredi, S.K., and Buck, K.R., 2001, Raman spectroscopic
286	and laser scanning confocal microscopic analysis of sulfur in living sulfur-
287	precipitating marine bacteria: Chemical Geology, v. 180, p. 3–18,
288	doi:10.1016/S0009-2541(01)00302-3.
289	Peckmann, J., Bach, W., Behrens, K., and Reitner, J., 2008, Putative cryptoendolithic life
290	in Devonian pillow basalt, Rheinisches Schiefergebirge, Germany: Geobiology, v. 6,
291	p. 125–135, doi:10.1111/j.1472-4669.2007.00131.x.
292	Peckmann, J., Thiel, V., Reitner, J., Taviani, M., Aharon, P., and Michaelis, W., 2004, A
293	microbial mat of a large sulfur bacterium preserved in a Miocene methane-seep
294	limestone: Geomicrobiology Journal, v. 21, p. 247–255,
295	doi:10.1080/01490450490438757.

296	Roveri, M., Flecker, R., Krijgsman, W., Lofi, J., Lugli, S., Manzi, V., Sierro, F.J., Bertini,
297	A., Camerlenghi, A., de Lange, G.J., Govers, R., Hilgen, F.J., Hübscher, C., Meijer,
298	P.T., and Stoica, M., 2014, The Messinian Salinity Crisis: Past and future of a great
299	challenge for marine sciences: Marine Geology, v. 352, p. 25-58,
300	doi:10.1016/j.margeo.2014.02.002.
301	Rouchy, J.M., and Monty, C., 2000, Gypsum microbial sediments: Neogene and modern
302	examples, in Riding, R.E., and Awramik, S.M, eds., Microbial Sediments: Berlin,
303	Heidelberg, Springer-Verlag, p. 209–216.
304	Schopf, J.W., Farmer, J.D., Foster, I.S., Kudryavtsev, A.B., Gallardo, V.A., and
305	Espinoza, C., 2012, Gypsum-permineralized microfossils and their relevance for the
306	search for life on Mars: Astrobiology, v. 12, p. 619–633, doi:10.1089/ast.2012.0827.
307	Schopf, J.W., Kudryavtsev, A.B., Walter, M.R., Van Kranendonk, M.J., Williford, K.H.,
308	Kozdon, R., Valley, J.W., Gallardo, V.A., Espinoza, C., and Flannery, D.T., 2015,
309	Sulfur-cycling fossil bacteria from the 1.8-Ga Duck Creek Formation provide
310	promising evidence of evolution's null hypothesis: Proceedings of the National
311	Academy of Sciences of the United States of America, v. 112, p. 2087–2092,
312	doi:10.1073/pnas.1419241112.
313	Schulz, H.N., and Jørgensen, B.B., 2001, Big bacteria: Annual Review of Microbiology,
314	v. 55, p. 105–137, doi:10.1146/annurev.micro.55.1.105.
315	Teske, A., and Nelson, D.C., 2006, The genera Beggiatoa and Thioploca: Prokaryotes,
316	v. 6, p. 784–810, doi:10.1007/0-387-30746-X_27.

317	Ueshima, M., and Tazaki, K., 2001, Possible role of microbial polysaccharides in
318	nontronite formation: Clays and Clay Minerals, v. 49, p. 292-299,
319	doi:10.1346/CCMN.2001.0490403.
320	Vai, G.B., and Ricci Lucchi, F., 1977, Algal crusts, autochthonous and clastic gypsum in
321	a cannibalistic evaporite basin; A case history from the Messinian of Northern
322	Apennine: Sedimentology, v. 24, p. 211–244, doi:10.1111/j.1365-
323	3091.1977.tb00255.x.
324	Vasconcelos, C., McKenzie, J.A., Bernasconi, S., Grujic, D., and Tien, A.J., 1995,
325	Microbial mediation as a possible mechanism for natural dolomite formation at low
326	temperature: Nature, v. 377, p. 220–222, doi:10.1038/377220a0.
327	Warren, J.K., 2010, Evaporites through time: Tectonic, climatic and eustatic controls in
328	marine and nonmarine deposits: Earth-Science Reviews, v. 98, p. 217-268,
329	doi:10.1016/j.earscirev.2009.11.004.
330	Ziolkowski, L.A., Mykytezuch, N.C.S., Omelon, C.R., Johnson, H., Whyte, L.G., and
331	Slater, G.F., 2013, Arctic gypsum endoliths: a biogeochemical characterization of a
332	viable and active microbial community: Biogeosciences, v. 10, p. 7661-7675,
333	doi:10.5194/bg-10-7661-2013.
334	FIGURE CAPTIONS
335	Figure 1. Distribution of Messinian evaporites (gypsum and halite) in the Mediterranean
336	basin (after Lugli et al., 2010). PB—Piedmont basin.
337	
338	Figure 2. A: Outcrop view of the Banengo section (northwest Italy) with underlying pre-
339	Messinian salinity crisis marls (Pre-MSC) and three tilted Primary Lower Gypsum cycles

340	composed of shale (S) and gypsum. Arrows indicate upward gypsum growth direction. B
341	Gypsum twin showing the alternation of turbid and clear laminae within the re-entrant
342	angle. The turbid laminae are rich in filamentous fossils. C: The euryhaline diatom
343	Surirella sp. D: Gypsum twin with curved filaments aligned to the vertical growth bands
344	(solid lines). Lamination in the re-entrant angle is indicated by dotted lines. E:
345	Fluorescent filament with small opaque pyrite inclusions. F: Hollow filamentous fossils
346	within gypsum. G: Isolated filament; a sequence of cellular compartments (outlined by
347	dashed lines) can be recognized. H: External surface of an isolated filament with a honey
348	comb structure. I: Isolated filament coated by dolomite microcrystals. J: Detail of I:
349	rounded dolomite microcrystals. B-D and F are plane-polarized light photomicrographs;
350	E is UV-light photomicrographs; G-J are scanning electron microscopy images.
351	
352	Figure 3. From the bottom to the top, Raman spectra of gypsum with filaments, pyrite
353	(rectangles), pyrite with polysulfide (circle), and carbonaceous material (dotted
354	rectangles).
355	
356	<sup>1</sup> GSA Data Repository item 2015 xxx, sampling, methodology, minerochemical and
357	XRD data of Messinian filamentous fossils (Table DR1 and Figures DR1-DR4) is
358	available online at www.geosociety.org/pubs/ft2015.htm, or on request from
359	editing@geosociety.org or Documents Secretary, GSA, PO Box 9140, Boulder, CO,
360	80301, USA.
361	
362	



Dela Pierre et al. Fig. 1 jpeg.

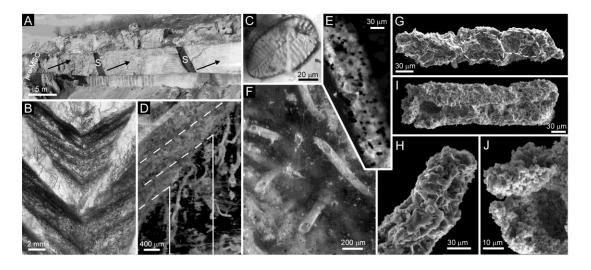


Fig. 2

376 1008 1366j \[ \overline{1366j} \] \[ \overline{17607j} \] \]

364

365

Dela Pierre et al Fig. 3 jpeg.